Journal Pre-proof

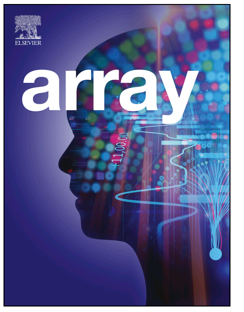

Extension of luminance component based demosaicking algorithm to 4- and 5-band multispectral images

Norbert Hounsou, Amadou T. Sanda Mahama, Pierre Gouton

PII: S2590-0056(21)00035-7

DOI: https://doi.org/10.1016/j.array.2021.100088

Reference: ARRAY 100088

To appear in: *ARRAY*

Received Date: 18 March 2021

Revised Date: 3 August 2021

Accepted Date: 24 August 2021

Extension of Luminance Component Based Demosaicking Algorithm to 4- and 5-band Multispectral Images

Norbert Hounsou[a], Amadou T. SANDA MAHAMA[a,*] and Pierre Gouton[b]

[a] University of Abomey-Calavi, Institute of Mathematics and Physics Sciences, Dangbo, Bénin**; secretariat@imsp-uac.org**
[b] University of Burgundy, Laboratoire Le2i; Dijon, France; ed.spim.dijon@ubfc.fr
* Correspondence: amadou.sanda@imsp-uac.org; Tel.: +229-95-05-33-43 (A.T.S. M.)

A B S T R A C T

Multispectral imaging systems are currently expanding with a variety of multispectral demosaicking algorithms. In this paper, we propose a powerful multispectral image demosaicking method that focuses on the G band and luminance component. We first identified a relevant 4-and 5-band multispectral filter array (MSFA) with the dominant G-band and then proposed an algorithm that consistently estimates the missing G values and other missing components using a convolution operator and a weighted bilinear interpolation algorithm based on the luminance component. Using the considered MSFA patterns, we also demonstrated that our algorithm outperforms existing approaches both visually and quantitatively in terms of the PSNR and SSIM.

Keywords:

Multispectral filter array
Luminance component
Demosaicking algorithm
Convolution
Weighted bilinear interpolation.

1. Introduction

Multispectral images are made of more than three bands. The higher the number of bands, the more information that is available and the more useful the image is [1, 2]. The MSFA imaging system is still a subject of considerable research and is still under development.

Multispectral image acquisition systems can be classified into three types [3]:

- multi-camera systems that capture images in a single shot using several cameras with different filters, thereby making the system quite complicated because a perfect alignment of several different cameras is required [4];
- single-camera multi-shot systems that capture images with a high spectral resolution but require multiple shots to obtain images with a high-speed lighting system for real-time imaging [5]; and
- single-camera systems that overcome the problems of the first two categories of systems in terms of size, cost, and real-time imaging [6-8]. Examples of the latter are RGB cameras equipped with one of Bayer's well-known color filter arrays (CFAs).

To capture multispectral images with a single image capture system, a multispectral filter array (MSFA) inspired by digital cameras featuring a Bayer CFA is required. Therefore, the use of a single camera system involves the design of MSFA-selective spectral filters arranged in a periodic mosaic defined by a basic pattern [2, 7, 9-13]. However, owing to the lack of a standard MSFA, as in the case of color images with a Bayer CFA, it is difficult to design an optimal MSFA and thus develop a powerful demosaicking algorithm. Several algorithms have been proposed in the literature [1, 3, 7, 9, 10, 14-19] using different MSFAs and achieving an attenuated performance. Although the luminance component is important in an image, few algorithms have explicitly used it in their demosaicking process [18].

In this paper, we have identified a 4- and 5-band MSFA and proposed a luminance component-based multispectral demosaicking algorithm (LCBD) that estimates the missing G component at each pixel by applying a convolution method, and the other components missing at each pixel using a luminance component. This paper is organized as follows: In the second section, we review the multispectral imaging systems proposed in the literature, and in the third section, we describe the actual proposed algorithm. The results and discussion are presented in the fourth Section.

2. State-of-the-art demosaicking techniques for multispectral image

For the implementation of multispectral image demosaicking techniques, the design of an optimal MSFA and an efficient demosaicking algorithm are two fundamental processes for the reconstruction of a full-resolution multispectral image that best limits the presence of artifacts. Several related proposals have been made in the literature.

2.1 Approaches to the design of the MSFA

Although Bayer's CFA was unanimously approved for use with color images, this is not the case with multispectral images. Numerous MSFA patterns have also been proposed [6]. For example, Miao et al. proposed a generic method for the design of MSFAs based on a binary tree, considering the probability of occurrence of each spectral band [10, 14]. The MSFA is generated based on the number of spectral bands and their appearance probabilities. Many of the recently proposed MSFAs have been inspired by this generic method. In addition, Monno et al. [7] proposed a 5-band MSFA pattern based on the high-density requirement of the G-band, as with Bayer's CFA, and their proposal was applied by Jaiswal et al. in their multispectral demosaicking algorithm [20]. Bangyong et al. also proposed a 4-band MSFA pattern [18] with the same probability of occurrence for each band and a 9-band MSFA [19] in which one band is dominant and the other bands with equal probability of occurrence are arranged in 4 × 4 patterns. Brauers and Aach [11] implemented a six-band MSFA in a 3 × 2 pattern to speed up the linear interpolation. Aggarwal and Majumdar proposed another simple MSFA by arranging four diagonally distributed filters [21] and then another random MSFA pattern [22], where each channel has the same probability of occurrence. Noting that the number of bands is inversely proportional to the spatial correlation, Shrestha et al. [23] proposed a particular MSFA pattern for a spectral reconstruction and estimation of the reflectance spectra. To find the best compromise between spatial and spectral resolution, Yasuma et al. designed a seven-band MSFA composed of three primary and four secondary color filters [12]. To overcome the difficulties in combining the spectral resolution and spatial correlation in multispectral imaging systems, Mihoubi et al. proposed a 16-band MSFA without dominant bands [2].

Several proposals have also been made for imaging systems involving the visible and near infrared (NIR) domains. Hershey and Zhang [24] designed a multispectral camera based on a 4-band MSFA with three color bands and a near-infrared band. Lu et al. [38] proposed an MSFA pattern as an optimization problem in the space domain by providing an iterative procedure to search locally for the optimal solutions. In addition, Kiku et al. [25] proposed a modified Bayer CFA pattern in which the additional fourth band was weakly sampled and arranged in a slightly tilted square grid. Indeed, their approach is based on the assumption that there is no correlation between the RGB and additional bands. The so-called Hybrid CFA still maintains a high density of the G band. Lapray et al. [6] defined two MSFA patterns with a periodic spatial distribution corresponding to two different approaches. One approach favors spatial information, and the other favors spectral information. For remote sensing applications, Mercier et al. [26] examined the usefulness of the design of an MSFA instantaneous sensor. These different MSFAs have been used in several multispectral demosaicking algorithms.

2.2 Review of the MSFA demosaicking algorithms

Demosaicking is one of the most delicate tasks in a multispectral imaging system. Numerous demosaicking algorithms have been proposed based on an extension of a classical CFA algorithm [27, 28]. Miao et al. [9] proposed a generic multispectral demosaicking method that interpolates each missing band using edge correlation information. The method first determines the interpolation order of the different spectral bands, followed by the interpolation order of the pixel locations for each spectral band. Finally, an interpolation algorithm that uses the edge correlation information is applied. By exploring the spatial and spectral correlation information in an interpolation of the missing bands, Aggarwal et al. [29] proposed a linear demosaicking technique that applies linear filtering on a raw MSFA image with a kernel whose parameters are determined through training. In [12], the MSFA is composed of three primary and four secondary color filters, and a low-pass filter in the Fourier domain is used to reconstruct the primary color, whereas the principle of a constant channel difference and residual interpolation by means of the correlation between channels is exploited to reconstruct the secondary spectral bands.

In [11], Brawers and Aach proposed a linear algorithm in which the conventional color difference is first smoothed. The authors initially compute the sparse channel difference for each spectral band, and a fully defined channel difference is then estimated at each spectral band through a convolution of the previous sparse channel difference with a low-pass filter, which is a smoothing operation. Finally, a weighted bilinear interpolation is applied to the channel difference estimated to obtain the band at each pixel. Mizutani et al. [39] proposed an improvement of Brawers and Aach's method by iterating the process a certain number of times depending on the neighborhood considered. The interpolation was then extended to a multispectral approach. Wang et al. [13] extended classical median filtering to MSFA demosaicking. The spectral response of the filtering is derived from the input vectors by estimating the missing value at one band with another value close to the same or another band. In [30], the authors extended a CFA method based on the discrete wavelet transform to multispectral demosaicking by estimating the low-and high-frequency components of the missing bands. Later, they proposed a generic MSFA demosaicking algorithm based on linear interpolation, which combines the linear minimum mean square error (LMMSE) technique and the residual interpolation method [31]. Monno et al. [3, 7, 16, 17, 32] also proposed a series of demosaicking algorithms for a 5-band MSFA with a dominant G-band with a probability of occurrence of 50%. The first of these algorithms [3] uses an adaptive kernel that is estimated directly from a raw MSFA image and applied to an adaptive Gaussian oversampling to generate a guide image from the G-band data. The technique of joint bilateral adaptive oversampling is applied to both the guide image and the data of each spectral band to obtain the reconstructed image. In [16], the authors improved this method by using a guide filter, which is an excellent structure preservation filter that performs a linear transformation of a given guide image to interpolate the missing bands. The authors used a residual interpolation to generate a guide image for a structure preserving interpolation [17] and proposed an adaptive residual interpolation by adaptively combining two algorithms based on residual interpolation and selecting an appropriate number of iterations for each pixel [32]. The authors then developed several guided images that were used in the interpolation of different bands [7]. Jaiswal et al. [20] also used the high-frequency component of the G-band to interpolate the other bands based on an inter-band correlation analysis. In addition, Mihoubi et al. [2] proposed a 16-band MSFA algorithm based on a pseudo-panchromatic image (PPI), which is estimated by applying an averaging filter to the raw image and then adjusted such that the PPI values are correlated. The difference between each available value of the adjusted raw image and PPI is calculated. The calculated local directional weights are then used to estimate the fully defined difference using an adaptive weighted bilinear interpolation. Each band is finally estimated by adding a PPI and the difference. In [33], the authors proposed a method that uses spatial and spectral correlations to estimate the missing bands. Recently, Amba et al. [34] extended the algorithm based on linear minimum mean square errors for RGB color to multispectral demosaicking by applying a linear operator that minimizes the mean square error between the reconstructed image and the original raw image. This linear operator multiplied by the MSFA image provides an estimate of the reconstructed image. In [18], a method of applying directional interpolation along the edges of an image was proposed. In this method, the image edges are calculated from the raw image to define the direction interpolation with the neighbors. Considering the features of the filter arrays, image edges, and a constant hue, the missing bands per pixel were recovered from the existing bands. Then, the image is separated into high-and low-frequency components by applying a wavelet transform, and the high-frequency images that are highly correlated are modified using luminance information to refine the demosaicked image. In [19], a multispectral algorithm that estimates the missing dominant band at each spatial position with a weighted average of the neighboring values of the dominant band was described. The dominant band reconstructed at different spatial positions is then used as a guided image to estimate all other missing bands using the guided filter and a residual interpolation.

Table 1. Comparison table of existing methods

Authors	Contributions	Limitations	References	Dates of Publication
Miao et al.	- Generic MSFA based on binary tree - Generic multispectral demosaicking - Spatial and spectral correlation exploitation - Utilisation of edge correlation information	- Probabilies occurrence of spectral bands are in order ½, ¼, or 1/8 which are restrictive and cannot be arbitrary - The performance of edge sensing interpolation is limited	[9]	November 2006
Brauers et Aach	- Periodic 6-band MSFA - Spectral correlation exploitation - Bilinear interpolation of color difference using convolution - Applicable to generic MSFA	Not taken into account of degree of cross-correlation between the demosaicked spectral bands	[11]	October 2006
Yasuma et al.	- 7-band MSFA with three primary and four secondary color filters - Linear interpolation with best compromise among spatial resolution, spectral resolution and dynamic range	Insufficient performance	[12]	September 2010
Wang et al.	- Interpolation based on discrete wavelet transform - Low-frequency and high-frequency components are interpolated differently	The performance depends a lot on the spectral correlation	[30]	September 2013
	- LMMSE and residual interpolation combination using Wiener interpolation - Low dependence on the MSFA pattern	Sensitive to noise	[31]	July 2014
Mizutani et al.	- Improvement Brauers method by an iterative color difference algorithm	Higher the number of spectral band, higher the iteration and more complex the algorithm	[39]	December 2014
Aggarwal et al.	- Periodic diagonal MSFA - Weighted linear interpolation based on prior learning of weights	Limited performance for random MSFA	[29]	June 2014
Monno et al.	- Generic 5-band MSFA with dominant G-band - Guided filtering interpolation	Insufficient performance	[16]	January 2012
	- Generic 5-band MSFA with dominant G-band - Adaptative residual interpolation	Some appearances artefacts in the reconstruct image	[32]	December 2017
Jaiswal et al.	- Using Generic MSFA of Monno et al. - Algorithm based on inter-band correlation using frequency domain analysis	The performance depends on spectral correlation	[20]	February 2017
Amba et al.	-LMMSE extension for 8-band MSFA algorithm	Limited performance in the object edge	[34]	June 2017
Mihoubi et al.	- 16-band MSFA algorithm - Algorithm based on the pseudo-panchromatic image estimation	The complexity of the method	[2]	April 2017
Sun et al.	- Generic 4-band MSFA uniform - Method based on constant hue and wavelet transform	Limited performance for random MSFA	[18]	April 2018

- Generic 9-band MSFA with dominant G-band - Guided filtering and residual interpolation	Processing limits information to edge	[19]	January 2020

3. Proposed multispectral demosaicking system

3.1 Selected MSFA pattern

In multispectral single-sensor imaging, an increase in the number of spectral bands weakens the spatial correlation. To preserve the spectral coherence and spatial uniformity, we generate the MSFA using a generic method based on a binary tree [9,10,14,15]. With this method, the MSFA is generated by recursively dividing the checkerboard pattern based on a binary tree. The binary tree is defined by the number of spectral bands and the sampling densities of each spectral band, which are considered as parameters. The MSFA is formed by assigning each spectral band to the leaf of the binary tree.

In our case, for the 4- and 5-band MSFA patterns identified (see Figs. 1 and 2), we assigned higher sampling densities in the following order: G, R, and B-O for the 4-band MSFA and G, R-B-O-C for the 5-band MSFA, respectively. Table 2 shows the probability of the occurrence of spectral bands in each MSFA pattern.

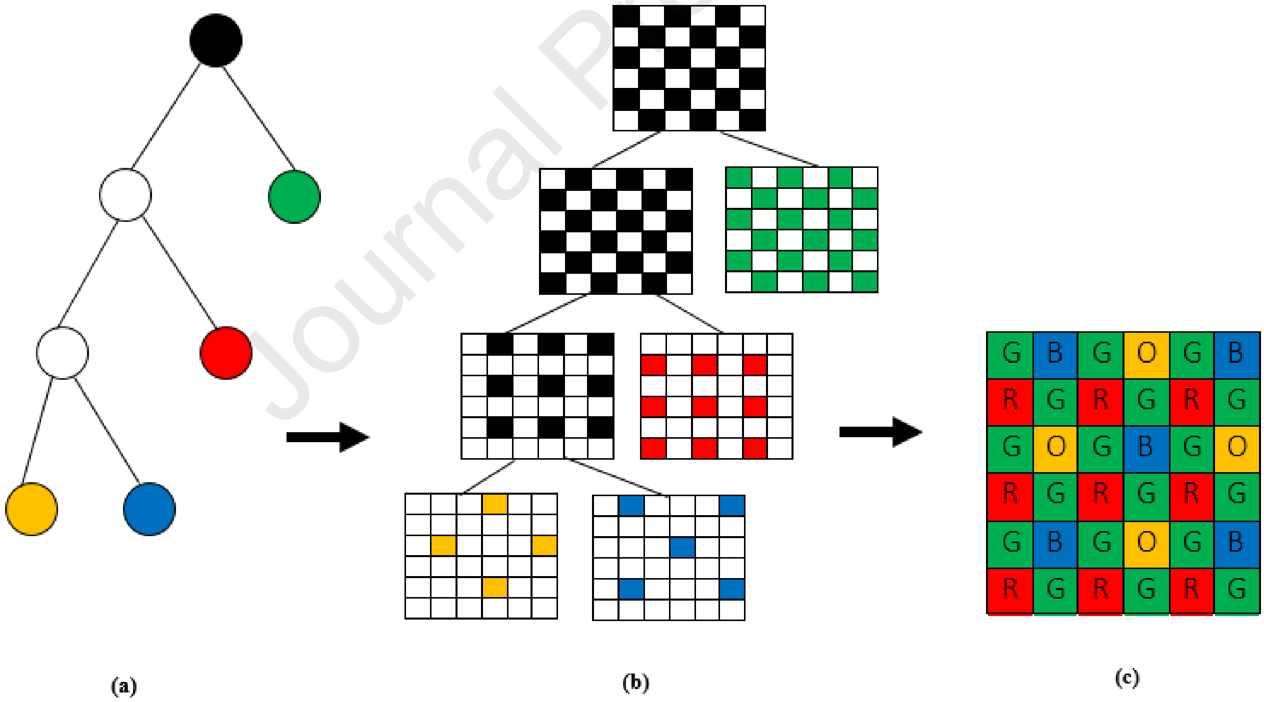

Fig. 1. 4-band MSFA configuration preceded by binary tree: (a) Binary tree considering appearance probabilities (b) Decomposition and subsampling processes (c) MSFA configuration.

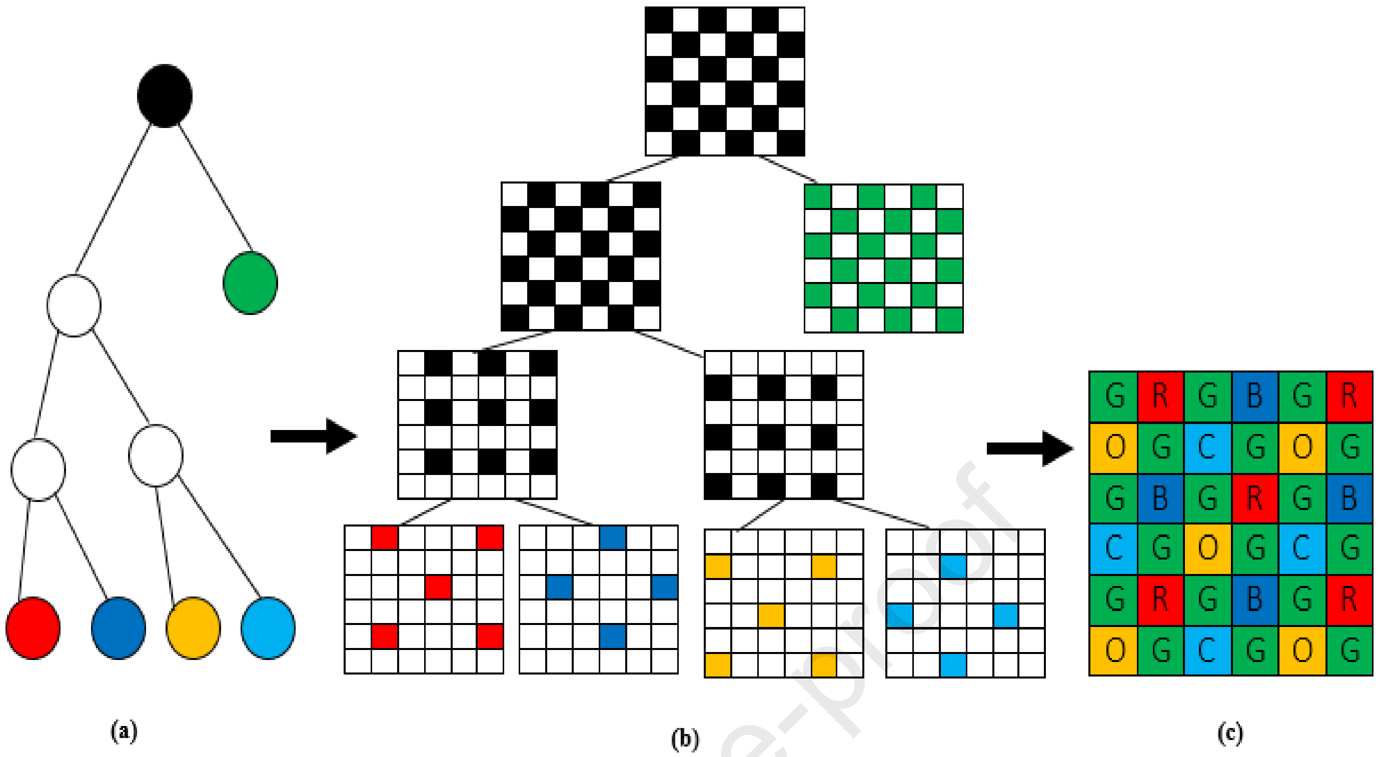

Fig. 2. 5-band MSFA configuration preceded by binary tree: (a) Binary tree considering appearance probabilities (b) Decomposition and subsampling processes (c) MSFA configuration.

Table 2. Probability occurrence of spectral bands

MSFA	Spectral Band				
	R	G	B	O	C
4-band	1/4	1/2	1/8	1/8	-
5-band	1/8	1/2	1/8	1/8	1/8

3.2 Estimating multispectral luminance

A multispectral image is represented by an array of M rows, N columns, and P spectral channels. At each spatial location (x, y), several spectral components (S_p) are defined by

$$S_p(x,y) = \int_{\lambda} L(x,y,\lambda)\phi_p(\lambda)d\lambda \quad (1)$$

where $L(x,y,\lambda)$ is the spectrally dependent irradiance at each location, $\phi_p(\lambda)$ is the spectral sensitivity function for a given sensor response (Fig.3), and λ is the wavelength [6].

Let $I_{MSFA}(x,y)$ be a raw multispectral digital image from a single sensor. $I_{MSFA}(x,y)$ is a mosaic image with one channel per pixel and can be represented by

$$I_{MSFA}(x,y) = \sum_p S_p(x,y)Z_p(x,y) \quad (2)$$

where $\mathbf{Z_p}(\mathbf{x},\mathbf{y})$ are the orthogonal functions of dimension P and take values of 1 or 0 if channel p is present or not at the location $(\mathbf{x},\mathbf{y})$, respectively.

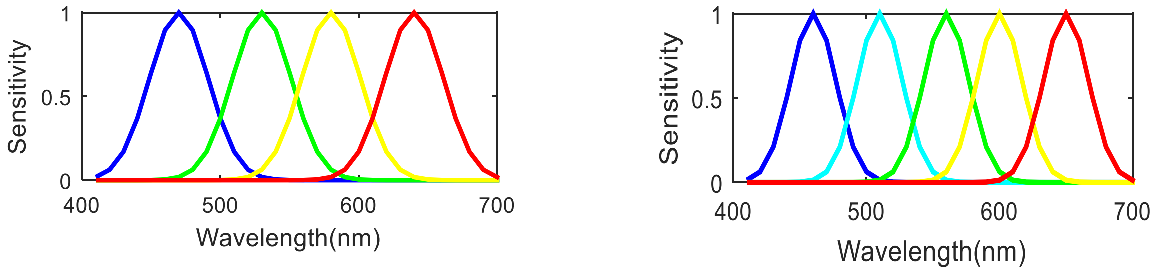

Fig. 3. Spectral sensitivity of the 4- (left) and 5-band (right) filters

In frequency domain, referring to the MSFA in [18], an N-band single-sensor spectral imaging process raw data is expressed as follows:

$$I_{MSFA}(x, y) = \sum_p S_p(x, y) m_p(x, y) \tag{3}$$

where $m_p(x, y), (p = R, G, B, O, C)$ are the modulation functions at position (x, y) whose expressions depend on the MSFA pattern. Applied to our 4- and 5-band MSFA patterns chosen in Figs. 1(c) and 2(c), these modulation functions can be expressed as follows:

$$\begin{cases} m_R(x, y) = (1 + \cos(\pi x))(1 + \cos(\pi y))/4 \\ m_G(x, y) = (1 + \cos(\pi x)\cos(\pi y))/2 \\ m_B(x, y) = (1 - \cos(\pi x))(1 + \cos(\pi y))/8 \\ m_O(x, y) = (1 - \cos(\pi x))(1 - \cos(\pi y))/8 \end{cases} \tag{4}$$

For 4-band MSFA

$$\begin{cases} m_R(x, y) = (1 + \cos(\pi x))(1 + \cos(\pi y))/8 \\ m_G(x, y) = (1 + \cos(\pi x)\cos(\pi y))/2 \\ m_B(x, y) = (1 - \cos(\pi x))(1 + \cos(\pi y))/8 \\ m_O(x, y) = (1 - \cos(\pi x))(1 - \cos(\pi y))/8 \\ m_C(x, y) = (1 + \cos(\pi x))(1 - \cos(\pi y))/8 \end{cases} \tag{5}$$

For 5-band MSFA

From equation (4) of 4-band MSFA, Eq. (3) becomes

$$I_{MSFA}(x, y) = \tfrac{1}{4}\left[R(x, y) + 2G(x, y) + \tfrac{1}{2}B(x, y) + \tfrac{1}{2}O(x, y)\right] + \tfrac{1}{4}\left[R(x, y) - \tfrac{1}{2}O(x, y)\right][\cos(\pi x) + \cos(\pi y)] + \tfrac{1}{4}\left[R(x, y) + 2G(x, y) - \tfrac{1}{2}B(x, y) + \tfrac{1}{2}O(x, y)\right]\cos(\pi x)\cos(\pi y) - \tfrac{1}{8}B(x, y)[\cos(\pi x) - \cos(\pi y)] \tag{6}$$

Let consider the following transformation:

$$\cos(\pi x) = \cos(\pi(x + y - y)) = \cos(\pi(x + y))\cos(\pi y) + \sin(\pi(x + y))\sin(\pi y). \tag{A}$$

Our MSFA pattern is such that the sum of the spatial coordinates x and y at G pixels in the MSFA image is even, then, $\cos(\pi(x + y)) = 1\,;\sin(\pi(x + y)) = 0.$ *(B)*

From (A) and (B), we have $\cos(\pi x) = \cos(\pi y)$. Therefore, at G pixels, Equation (6) becomes

$$I_{MSFA}(x, y) = \tfrac{1}{4}\left[R(x, y) + 2G(x, y) + \tfrac{1}{2}B(x, y) + \tfrac{1}{2}O(x, y)\right] + \tfrac{1}{4}\left[R(x, y) - \tfrac{1}{2}O(x, y)\right][\cos(\pi x) + \cos(\pi y)] + \tfrac{1}{4}\left[R(x, y) + 2G(x, y) - \tfrac{1}{2}B(x, y) + \tfrac{1}{2}O(x, y)\right]\cos(\pi x)\cos(\pi y) \tag{7}$$

This equation can be separated into two parts through

$$I_{MSFA}(x,y) = \tfrac{1}{4}\left[R(x,y) + 2G(x,y) + \tfrac{1}{2}B(x,y) + \tfrac{1}{2}O(x,y)\right] + \sum_{S=R,G,B,O} S(x,y)\tilde{m}_S(x,y) \tag{8}$$

Similarly, under the same conditions, the 5-band MSFA multispectral image can be written as

$$I_{MSFA}(x,y) = \tfrac{1}{8}\left[R(x,y) + 4G(x,y) + B(x,y) + O(x,y) + C(x,y)\right] + \tfrac{1}{8}\left[R(x,y) - O(x,y)\right]\left[\cos(\pi x) + \cos(\pi y)\right] + \tfrac{1}{8}\left[R(x,y) + 4G(x,y) + O(x,y) - B(x,y) - C(x,y)\right]\cos(\pi x)\cos(\pi y) \tag{9}$$

and (9) can be separated into two terms as

$$I_{MSFA}(x,y) = \tfrac{1}{8}\left[R(x,y) + 4G(x,y) + B(x,y) + O(x,y) + C(x,y)\right] + \sum_{S=R,G,B,O,C} S(x,y)\tilde{m}_S(x,y) \tag{10}$$

From equations (8) and (10), we obtain the following terms

$$L_{4\_MSFA}(x,y) = \tfrac{1}{4}\left[R(x,y) + 2G(x,y) + \tfrac{1}{2}B(x,y) + \tfrac{1}{2}O(x,y)\right] \tag{11}$$

$$L_{5\_MSFA}(x,y) = \tfrac{1}{8}\left[R(x,y) + 4G(x,y) + B(x,y) + O(x,y) + C(x,y)\right] \tag{12}$$

Equations (11) and (12) represent the luminance components at the G pixels, in the 4-and 5-band MSFA, and the other terms of equations (8) and (10) represent the chrominance components. In [35], a Gaussian low-pass filter with 11 × 11 support was used to estimate the luminance at each pixel of the CFA image. Lyan et al. [36] also showed the limitations of this filter and proposed a Gaussian low-pass filter with a 5 × 5 support to estimate the luminance at the G pixels of the CFA image because there is less overlap between the luminance and chrominance. Consequently, the complexity of the algorithm is reduced and the results are improved as much as possible. In our case, the condition of the spatial coordinates at G pixels reduces the overlap between the luminance and chrominance components and can avoid artifacts in the reconstructed multispectral image. Thus, we use a Gaussian low-pass filter with a 5 × 5 support in [36] to estimate the luminance component at the G pixels, and for other pixels, a Gaussian low-pass filter with 11 × 11 support was proposed in [35]. The chrominance components were obtained by the color difference.

3.3 Proposed multispectral demosaicking algorithm

The algorithm is a multistep approach and first estimates the missing G components.

3.3.1 G component missing estimation

To consider at the edges, we used the convolution method to estimate the missing green components with a symmetric 3 × 3 low-pass filter according to equation (13). Let $\hat{G}$ be the estimated G component at each pixel R, G, B, O, and C.

$$\hat{G}(x,y) = \sum_{i=1}^{m}\sum_{j=1}^{n} g(i,j)\, f(x-i, y-j) \tag{13}$$

The convolution kernel g is a low pass filter defined as

$$g = \tfrac{1}{4}\begin{pmatrix} 0 & 1 & 0 \\ 1 & 4 & 1 \\ 0 & 1 & 0 \end{pmatrix} \tag{14}$$

The matrix product f of $\breve{G}$ and I_{MSFA} allows an updating of the values of the different pixels at each spatial position before the convolution.

$$f(x, y) = \breve{G}(x, y) I_{MSFA} \tag{15}$$

The subsampling $\breve{G}$ of G band is obtained from MSFA (Figs. 1(c) and 2(c)) by filling in of each G pixel with a 1 the other pixels by zero:

$$\breve{G}(x, y) = \begin{cases} 1 & \text{in G pixel} \\ 0 & \text{otherwise} \end{cases} \tag{16}$$

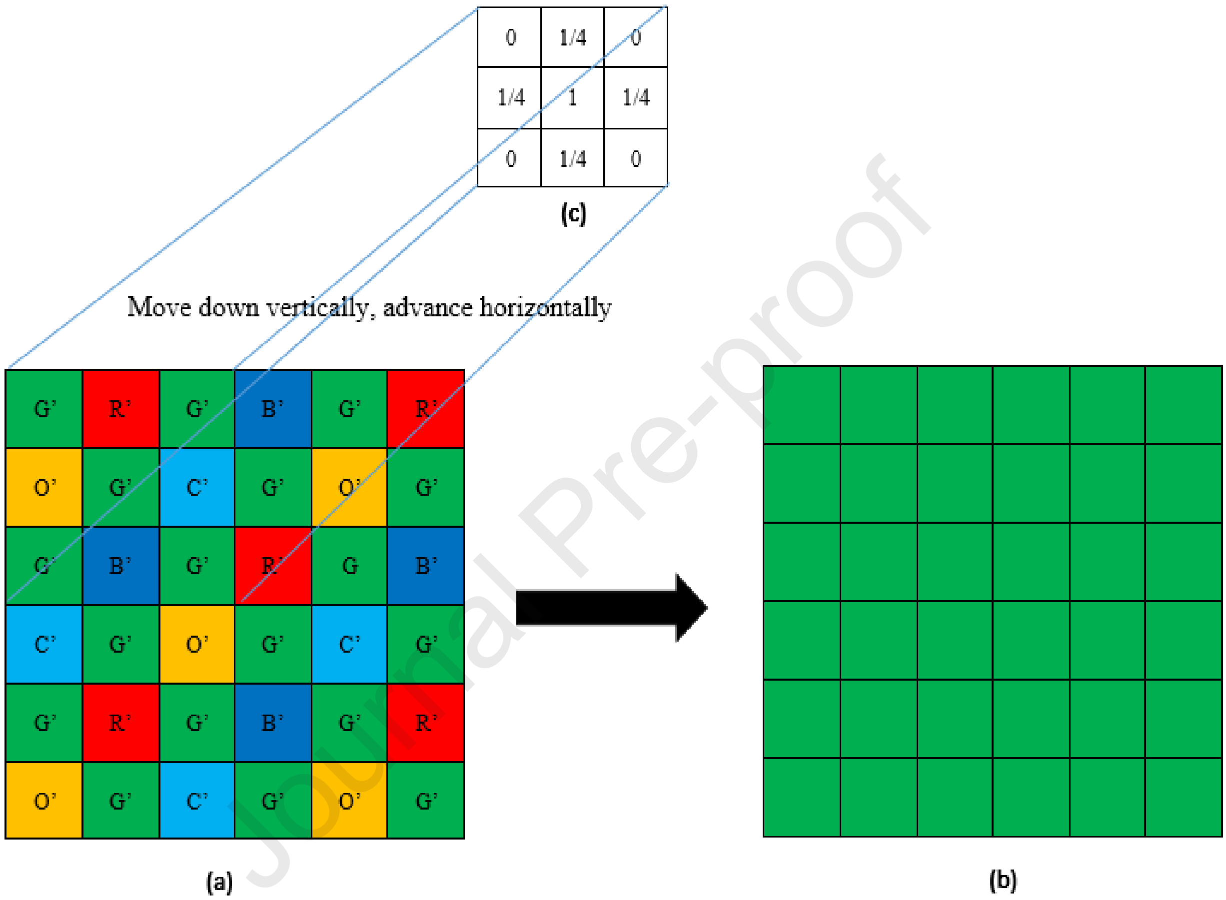

Fig.4. G band estimation using convolution method: (a) f matrix (b) G estimated values at each pixel (c) g convolution kernel

3.3.2 Other channels estimation at G pixels

After estimating the missing green bands at different pixels, each missing component, R, B, O, and C, at G pixels is determined through a bilinear interpolation of the color difference $R - \hat{G}$, $B - \hat{G}$, $O - \hat{G}$, and $C - \hat{G}$, respectively.

Referring to the 4-band MSFA (Fig. 1(c)), G pixels have red (R) neighbors in the horizontal or vertical direction. Therefore, we estimate R using

$$R(x, y) = \begin{cases} \mathrm{G(x,\ y)} + \frac{1}{2}(\mathrm{R(x,\ y-1) - G(x,\ y-1) + R(x,\ y+1) - G(x,\ y+1)}) & \text{if R in horizontal neighbors} \\ \mathrm{G(x,\ y)} + \frac{1}{2}(\mathrm{R(x-1,\ y) - G(x-1,\ y) + R(x+1,\ y) - G(x+1,\ y)}) & \text{if R in vertica l neighbors} \end{cases} \tag{17}$$

Moreover, the G pixels have similar B and O neighbors in the horizontal and vertical directions. Therefore, B and O were estimated in the same manner. In the horizontal direction, they occupy $(x, y-1)$, $(x, y+3)$, (first position), or $(x, y-3)$, $(x, y+1)$ (second position) of the G pixels. Next, we estimate B as follows:

$$B(x,y)=\begin{cases} G(x,y) + \frac{1}{2}(B(x,y-1) - G(x,y-1) + B(x,y+3) - G(x,y+3)) & \text{if } B \text{ in first position} \\ G(x,y) + \frac{1}{2}(B(x,y-3) - G(x,y-3) + B(x,y+1) - G(x,y+1)) & \text{if } B \text{ in second position} \end{cases} \quad (18)$$

In the vertical direction, B is estimated in the same way by inverting the index order.

For a 5-band MSFA (Fig. 2(c)), the same strategy is used to estimate the R, B, O, and C bands in the G pixels.

3.3.3 Other missing component estimation at other pixels

The other missing components R, B, O and C at the pixels C, O, B and R are estimated by the weighted sum of the color differences, where the weights are calculated on the basis luminance components according to the steps:

3.3.3.1 Multispectral luminance $\hat{\hat{\boldsymbol{l}}}(\boldsymbol{x},\boldsymbol{y})$ estimation

We estimate the luminance component $\hat{L}(x,y)$ at different pixels according to the methods described in section 3.2

3.3.3.2 Weight calculation

The estimated luminance $\hat{L}(x,y)$ is decomposed using a low-pass filter normalized as $H_0 = 1/8\,[1\ 3\ 3\ 1]$ and transposing $H_0{}'$ into the horizontal $\hat{L}_{HL}(x,y)$ and vertical $\hat{L}_{LH}(x,y)$ components, unlike the wavelets used in our previous article [27].

We calculated the energies of $\hat{L}_{HL}(x,y)$ and $\hat{L}_{LH}(x,y)$, denoting them as $e_{HL}(x,y)$ and $e_{LH}(x,y)$, respectively, and used them to compute the horizontal and vertical weights at each pixel:

$$W_h(x,y) = \frac{F * e_{HL}(x,y)}{F * e_{HL}(x,y) + F * e_{LH}(x,y)} \quad (19)$$

$$W_v(x,y) = \frac{F * e_{LH}(x,y)}{F * e_{HL}(x,y) + F * e_{LH}(x,y)} \quad (20)$$

where F is a spatial averaging kernel of 3×3 size.

$$F = \frac{1}{9}\begin{pmatrix} 1 & 1 & 1 \\ 1 & 1 & 1 \\ 1 & 1 & 1 \end{pmatrix} \quad (21)$$

The energies $e_{HL}(x,y)$ and $e_{LH}(x,y)$ are calculated as

$$e_{HL} = \left|\hat{L}_{HL}\right|^2 \qquad e_{LH} = \left|\hat{L}_{LH}\right|^2 \quad (22)$$

The red samples in the blue locations were estimated as follows:

$$\hat{R}(x,y) = B(x,y) + \frac{w_h(x,y)}{2}\left(\hat{D}_{RB}(x-1,y) + \hat{D}_{RB}(x+1,y)\right) + \frac{w_v(x,y)}{2}\left(\hat{D}_{RB}(x,y-1) + \hat{D}_{RB}(x,y+1)\right) \quad (23)$$

Where:

$$\hat{D}_{RB}(x,y) = \hat{R}(x,y) - \hat{B}(x,y) \quad (24)$$

The same strategy was applied to reconstruct the blue component in the red locations. This was the same for the other components. A block diagram of the proposed algorithm is shown in Fig.5.

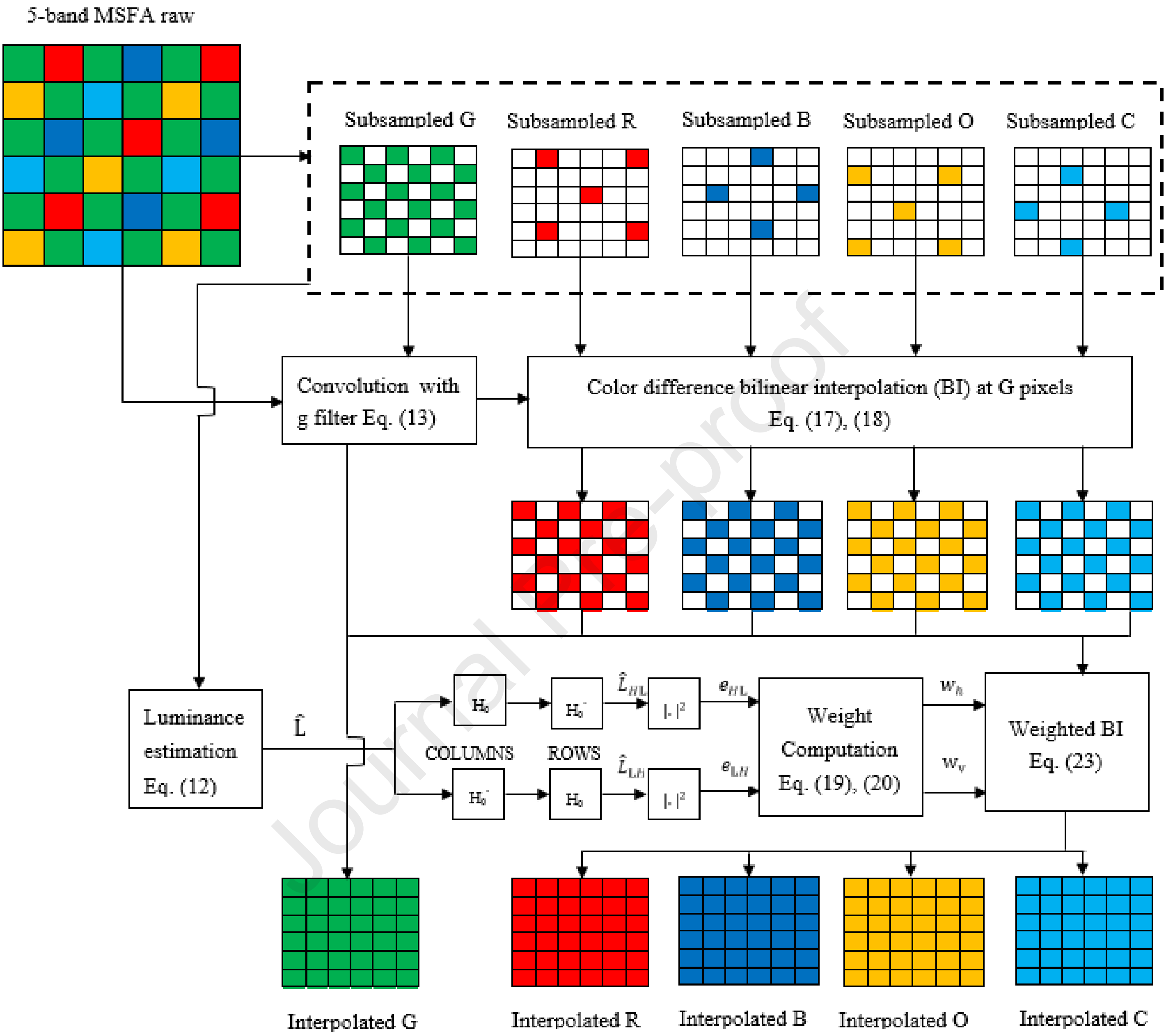

Fig. 5. Block diagram of the proposed algorithm

4. Results and discussion

In our experiments, we used 15 images from a cave dataset [37], in which multispectral images consist of 31-band multispectral images acquired under illuminant D65. The 31-band images were acquired every 10 nm at between 400 and 700 nm. The image size was 512×512 pixels. The CAVE dataset is often used as a standard multispectral image dataset.

To evaluate the performance of the proposed algorithm, we compared it with recent 4-band multispectral demosaicking methods, namely inter-band bilinear interpolation (IBBI) [28], generic binary tree edge sensing (BTES) [9], learned interpolation weights (LIW) [29], and directional filtering and wavelet transformation

(DFWF) [18]. In the case of 5-band multispectral demosaicking methods, the comparison is applied using the demosaicking algorithm based on adaptive spectral-correlation demosaicking (ASCD) [20], Practical One-Shot multispectral demosaicking (POS) [7], the BTES method [9], a guided filter (GF) [16], linear interpolation (LI) [31], and the iterative intensity difference (IID) [33]. Visual and objective evaluations were also conducted.

4.1. Visual performance evaluations

For evaluation purposes, we selected the statue, bead, and sponge images from the cave dataset. Fig. 6 shows the results of the R-band of the image *statue* for different algorithms. The images reconstructed by the different comparison algorithms appear sharper than those of the original image, but are highly blurred. The BTES, LI, and POS methods show an edge degradation; however, such problems are reduced with the GF, ASCD, and IID methods. However, the image reconstructed using the proposed method has almost the same sharpness as the original image, but with almost no edge distortion or blurring. Fig.7 shows the results of the G-band of the image *bead* of the different algorithms. As can be seen, the BTES and LI methods exhibit severe edge distortion and blurring. These distortions are also visible with the ASCD method but are less accentuated. With the GF, POS, and IID methods, blurring was noticeable. Our method presents slight edge distortions, but with an almost complete absence of blurring. In Fig.8, we show the results of the visual comparison of the O-band of the image *sponge* produced using the demosaicking algorithms. We see that the image reconstructed by the GF method appears sharper than the original image but with artifacts, whereas the image reconstructed by the ASCD method is less sharp but retains the edges. With the BTES, LI, and POS methods, the reconstructed images show artifacts, and the text is extremely unclear. Similarly, the performance of the IID method is insufficient compared with our approach in terms of the reconstructed image. By contrast, the image reconstructed by the proposed algorithm contains fewer distortions, and the text is clearer. Clearly, the same behavior was observed for the B- and C-bands.

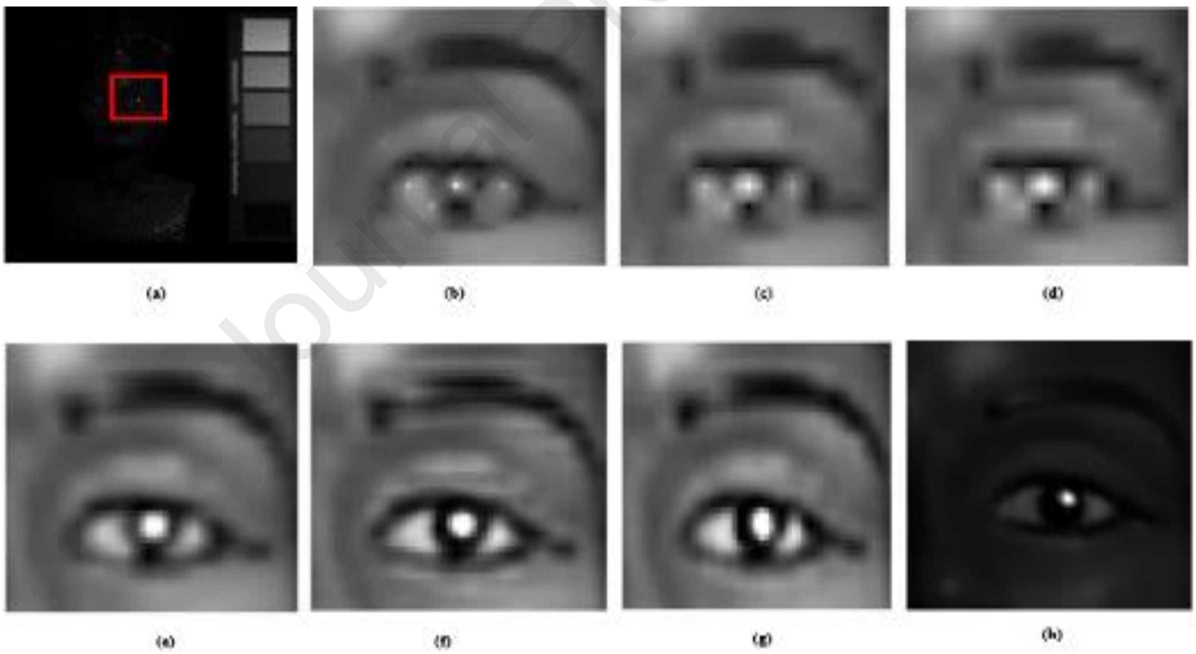

Fig. 6. Visual comparison of R band of statue image: (a) Original R Band, (b) GF, (c) BTES, (d) LI, (e) ASCD, (f) POS, (g) IID, and (h) proposed approach for 5-band MSFA.

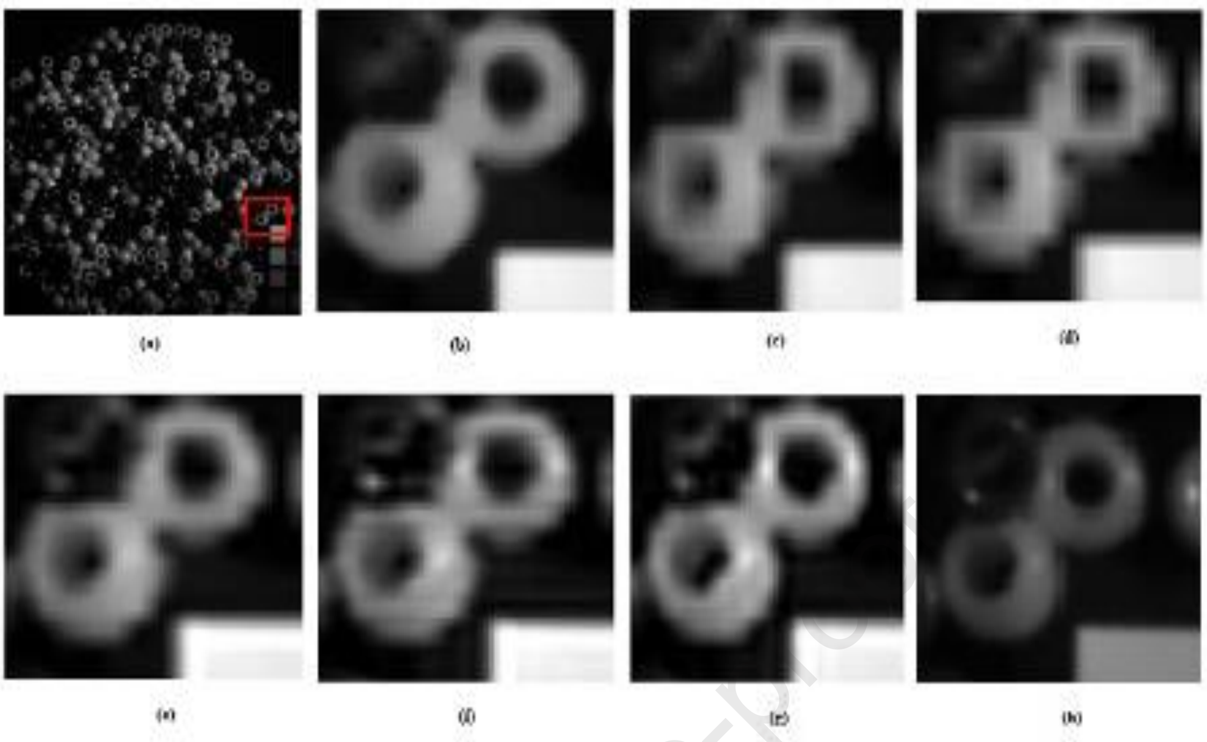

Fig. 7. Visual comparison of G band of bead image: (a) Original G Band, (b) GF, (c) BTES, (d) LI, (e) ASCD, (f) POS, (g) IID, and (h) proposed approach for 5-band MSFA.

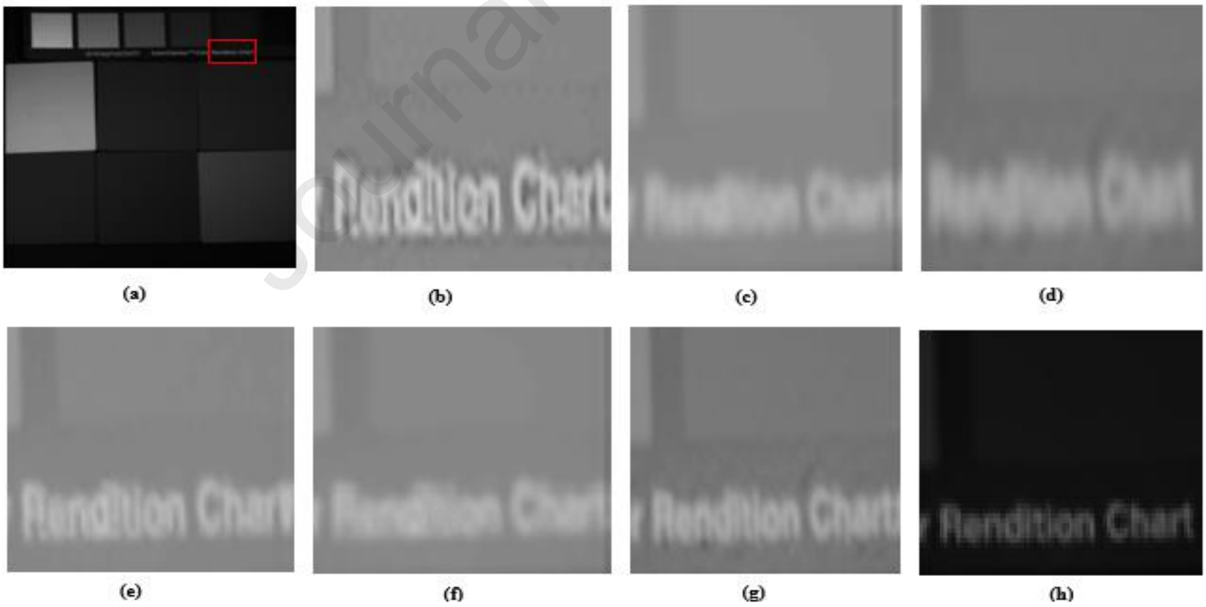

Fig.8. Visual comparison of O band of sponge image: (a) Original G Band; (b) GF; (c) BTES; (d) LI; (e) ASCD; (f) POS; (g) IID;(h) proposed approach for 5-band MSFA.

4.2. Quantitative performance evaluations

To quantitatively assess the objective performance of the proposed 4- and 5-band MSFA algorithms, we used the peak signal-to-noise ratio (PSNR) and structural similarity index (SSIM) metrics as described in [18, 31], calculated from the original and demosaicked images.

The average results obtained from the proposed algorithm through the PSNR and SSIM values are recorded in Tables 3 and 4 for the 4-band MSFA and in Tables 5 and 6 for the 5-band MSFA. The results of the other algorithms are provided in [20].

Table 3. PSNR results of 4-band MSFA demosaicking algorithms

Images	IBBI[28]	BTES[9]	LIW[29]	DFWF[18]	LCBD
Balloons	45.67	42.03	38.07	46.94	**50.19**
Feathers	37.43	35.15	33.19	39.44	**41.38**
Pompoms	41.40	38.46	30.06	41.29	**43.14**
Toys	43.90	42.71	34.54	43.43	**44.52**
Beads	32.31	30.75	26.48	**33.21**	31.68
Cloth	30.86	28.53	29.99	31.36	**34.29**
Statue	42.75	40.63	37.81	**44.14**	38.14
Face	41.28	38.21	36.05	40.29	**42.71**
Flowers	42.87	39.11	36.07	38.43	**44.03**
Beans	35.04	32.62	30.68	**36.93**	35.26
Painting	31.99	30.89	31.02	34.86	**35.81**
Thread	38.62	36.34	37.77	43.30	**41.22**
Superballs	43.59	41.79	39.47	**44.93**	39.60
Food	42.73	40.08	37.37	**43.26**	40.65
Watercolors	34.49	32.25	27.05	36.15	**45.70**
Average	38.99	36.64	33.71	39.73	**40.55**

Table 4. SSIM results of 4-band MSFA demosaicking algorithms

Images	IBBI[28]	BTES[9]	LIW[29]	DFWF[18]	LCBD
Balloons	0.9012	0.9110	0.9025	0.9017	**0.9980**
Feathers	0.9576	**0.9934**	0.9902	0.9907	0.9870
Pompoms	0.9228	**0.9928**	0.9905	0.9898	0.9852
Toys	0.9657	**0.9983**	0.9972	0.9972	0.9917
Beads	0.8900	0.8857	0.8758	0.8823	**0.8903**
Cloth	0.9011	0.8670	0.8677	0.8862	**0.9272**
Statue	0.8816	0.8727	0.8849	0.8828	**0.9776**
Face	0.9924	0.9972	**0.9983**	0.9970	0.9939
Flowers	0.9663	**0.9958**	0.9946	0.9929	0.9859
Beans	0.9539	0.9864	**0.9911**	0.9835	0.9500
Painting	0.9415	0.9393	0.9833	0.9625	0.9231
Thread	0.9818	0.9888	**0.9969**	0.9942	0.9812
Superballs	0.9763	**0.9968**	0.9935	0.9952	0.9680
Food	0.8821	0.8864	0.8827	0.8639	**0.9688**
Watercolors	0.9739	0.9848	**0.9934**	0.9831	0.9857
Average	0.9393	0.9531	0.9562	0.9535	**0.9676**

Table 5. Average PSNR results of 5-band MSFA demosaicking algorithms

	Cave Dataset					
Algo.	**Spectral Band**					**Mean**
	R	**G**	**B**	**O**	**C**	

ASCD[20]	**45.81**	47.85	44.94	45.20	44.60	**45.68**
POS [7]	45.36	48.06	43.96	44.75	**44.69**	45.36
BTES[9]	42.60	46.54	40.46	39.41	37.84	41.37
GF [16]	44.61	47.65	43.31	42.13	41.25	43.79
LI [31]	43.79	47.05	41.05	40.65	39.12	42.33
IID [33]	44.10	46.31	43.34	43.12	42.52	43.87
LCBD	45.62	**50.36**	**48.74**	**47.53**	35.13	45.48

Table 6. Average SSIM results of 5-band MSFA demosaicking algorithms

Cave Dataset						
Algo.	**Spectral Band**					**Mean**
	R	**G**	**B**	**O**	**C**	
ASCD[20]	0.9841	0.9917	0.9856	0.9865	0.9821	0.9860
POS [7]	0.9831	0.9922	0.9822	0.9840	0.9825	0.9848
BTES[9]	0.9724	0.9801	0.9710	0.9610	0.9524	0.9674
GF [16]	0.9805	0.9910	0.9801	0.9770	0.9790	0.9815
LI [31]	0.9780	0.9889	0.9791	0.9671	0.9612	0.9749
IID [33]	0.9795	0.9874	0.9802	0.9701	0.9807	0.9796
LCBD	**0.9899**	**0.9946**	**0.9902**	**0.9897**	**0.9908**	**0.9910**

The best scores in the tables are in bold, and our MSFA pattern is not the same as that of the comparison methods. According to the results in Table 3, our proposed 4-band MSFA algorithm outperformed the other methods for 10 out of 15 images used in the Cave dataset in terms of the PSNR, achieving the best average PSNR value. This is followed by the DFWF method, which shows good scores for five of the images. As shown in Table 4, for the SSIM values, our method presents better results with five images and the best average SSIM value, followed by the BTES method, which presents good results with six images but a lower mean SSIM value than our approach. In general, the 4-band MSFA method proposed in this study is better than all other methods in terms of both the PSNR and SSIM.

Regarding the mean PSNR and SSIM of the proposed 5-band MSFA algorithm in Tables 5 and 6, our algorithm outperformed the others with three bands, i.e., G, B, and O, in terms of the PSNR, but with a slightly lower mean value, which is very close to the highest mean value of the ASCD method. This can be explained by the fact that the convolution technique used to estimate the dominant band considers the details of the edge where the inter-channel correlation is sufficiently high, which is not the case for the other bands, notably, the band C. However, in terms of the SSIM, the proposed method outperformed all other approaches. Globally, our algorithm has a high objective performance compared to the methods we selected from the recent literature.

5. Conclusion

In this paper, we propose a multispectral demosaicking algorithm that exploits a convolution method used to estimate the G-band and the luminance component to estimate the other missing bands of a single sensor image. To generate the identified MSFA as a function of the required density in the G-band, we used the generic Benary tree method. To extract this luminance component at the green pixels, we used a 5 × 5 Gaussian low-pass filter, and for the other components we applied an 11 × 11 Gaussian low-pass filter. The results of the tests carried out on the selected filters show that the proposed algorithm is more powerful than the existing approaches, both visually and in terms of objective measurements. In our future work, we will study the application of these results in areas such as agriculture, medicine, and other fields. Extensive studies will be undertaken to provide a general extension of the proposed algorithm to more than five image bands. In addition, the MSFAs upon which our study is related are rectangular, and we plan to explore the efficiency of hexagonal MSFAs.

Author Contributions

"Conceptualization, Norbert H., Amadou T. S. M. and Pierre G.; methodology, Norbert H., Amadou T. S. M. and Pierre G.; software, Norbert H. and Amadou T. S. M. ; validation Amadou T. S. M. and Pierre G..; formal analysis, Norbert H., Amadou T. S. M. and Pierre G.; investigation, Norbert H., Amadou T. S. M. and Pierre G.; resources, Norbert H., Amadou T. S. M. and Pierre G.; data curation, Norbert H. and Amadou T. S. M..; writing—original draft preparation, Norbert H. and Amadou T. S. M.; writing—review and editing, Norbert H. and Amadou T. S. M.; visualization, Norbert H., Amadou T. S. M. and Pierre G.; supervision, Amadou T. S. M. and Pierre G.; project administration, Amadou T. S. M. and Pierre G..; funding acquisition, Pierre G.

Acknowledgments

Thanks to all those who, from near or far, have contributed to the creation of this work.

Conflicts of Interest

The authors declare no conflict of interest.

REFERENCES

[1] S. Mihoubi, O. Losson, B. Mathon, L. Macaire, Multispectral demosaicing using intensity in edge-sensing and iterative difference-based methods, Interna. Conf. Signal-Image Tech. & Internet-Based Sys. (2016).

[2] S. Mihoubi, O. Losson, B. Mathon, L. Macaire, Multispectral demosaicing using pseudo-panchromatic image, IEEE Trans. Comput. Imaging, 3 (4) (2017) 982-995.

[3] Y. Monno, M. Tanaka, M. Okutomi, Multispectral demosaicking using adaptive kernel upsampling, IEEE Int. Conf. Image Process. (2011), 3218–3221.

[4] K. Ohsawa, H. Fukuda, T. Ajito, Y. Komiya, H. Haneishi, M. Yamaguchi, N. Ohyama, Six-band HDTV camera system for spectrum-based color reproduction. Imaging Sci. and Tech, 48 (2) (2004) 85-92

[5] C. Cui, H. Yoo, M. Ben-Ezra, Multi-spectral imaging by optimized wide band illumination, Comput. Visi. 86 (2-3) (2010) 140-151.

[6] P. J. Lapray, X. Wang, J. B. Thomas, P. Gouton, Multispectral filter arrays: Recent advances and practical implementation, Sensors, 14 (11) (2014) 21 626–21 659.

[7] Y. Monno, S. Kikuchi, M. Tanaka, M. Okutomi, A practical one shot multispectral imaging system using a single image sensor, IEEE Trans. Image Process. 24 (10) (2015) 3048-3059.

[8] J. B. Thomas, P. J. Lapray, P. Gouton, C. Clerc, Spectral Characterization of a Prototype SFA Camera for Joint Visible and NIR Acquisition, Sensors, 16 (2016) 993.

[9] L. Miao, H. Qi, R. Ramanath, W. E. Snyder, Binary tree-based generic demosaicking algorithm for multispectral filter arrays, IEEE Trans. Image Process. 15 (11) (2006) 3550–3558.

[10] L. Miao, H. Qi, The design and evaluation of a generic method for generating mosaicked multispectral filter arrays. IEEE Trans. Image Process. 15 (2006) 2780–2791.

[11] J. Brauers, T. Aach, A Color Filter Array Based Multispectral Camera. Group. G. C., Ed.; 12th Workshop, (2006).

[12] F. Yasuma, T. Mitsunaga, D. Iso, S. K. Nayar, Generalized Assorted Pixel Camera: Postcapture Control of Resolution, Dynamic Range, and Spectrum. IEEE Trans. Image Proc. 19 (2010) 2241–2253.

[13] X. Wang, J. B. Thomas, J. Y. Hardeberg, P. Gouton, Median filtering in multispectral filter array demosaicking, SPIE, Electronic Imag., Annu. Sympo., 8660 (2013) 86 600E–86 600E–10.

[14] L. Miao, H. Qi, W. E. Snyder, A generic method for generating multispectral filter arrays, Conf. ICIP, Conf. 5 (2014) 3343–3346.

[15] L. Miao, H. Qi, R. Ramanath, Generic MSFA mosaicking and demosaicing for multispectral cameras, SPIE, Digit. Photo. II. 6069 (2006) 606909.

[16] Y. Monno, M. Tanaka, M. Okutomi, Multispectral demosaicking using guided filter, SPIE, Electronic Imag. Annu. Sympos. 8299 (2012) 82 990O–82 990O–7.

[17] Y. Monno, D. Kiku, S. Kikuchi, M. Tanaka, M. Okutomi, Multispectral demosaicking with novel guide image generation and residual interpolation, IEEE, Interna. Conf. Image Process. ICIP, (2014) 645–649.

[18] B. Sun, N. Yuan, C. Cao, J. Y. Hardeberg, Design of four-band multispectral imaging system with one single-sensor, Future Gener. Comput. Syst. 86 (2018) 670–679.
[19] B. Sun, Z. Zhao, D. Xie, N. Yuan, Z. Yu, F. Chen, C. Cao, V. W. de Dravo, Sparse spectral signal reconstruction for one proposed nine-band multispectral imaging system, MSSP, (2020) 106627
[20] S. P. Jaiswal, L. Fang, V. Jakhetiya, J. Pang, K. Mueller, O. C. Au, Adaptive multispectral demosaicking based on frequency-domain analysis of spectral correlation, IEEE Trans. Image. Process. 26 (2) (2017) 953-968.
[21] H. K. Aggarwal, A. Majumdar, Multi-spectral demosaicing technique for single-sensor imaging, NCVPRIPG, (2013) 1–4.
[22] H. K. Aggarwal, A. Majumdar, Compressive Sensing Multi-Spectral Demosaicing from Single Sensor Architecture, IEEE, ChinaSIP, (2014) 9–13.
[23] R. Shrestha, J.Y. Hardenberg, R. Khan, Spatial arrangement of color filter array for multispectral image acquisition. Proc. SPIE (2011) 7875.
[24] J. Hershey, Z. Zhang, Multispectral Digital Camera Employing Both Visible Light and Non-Visible Light Sensing on a Single Image Sensor, U.S. Patent, 7 (460) (2008) 160.
[25] D. Kiku, Y. Monno, M. Tanaka, M. Okutomi, Simultaneous capturing of RGB and additional band images using hybrid color filter array, Proc. SPIE (2014) 9023.
[26] D. Menon, G. Calvagno, Demosaicing based on wavelet analysis of the luminance component, IEEE, Internat. Conf. Image Process. 2 (2007) 181-184.
[27] H. Norbert, T. S. M. Amadou, G. Pierre, J. B. Thomas, Comparative Study Of Biorthogonal Wavelets Accuracy In Demosaicing Algorithm Based On Wavelet Analysis Of Luminance Component, IS&T, 16 (2018) 365-367.
[28] S. Susan, D. Aneja, Edge Strength based Fuzzification of Colour Demosaicking Algorithms, Defence Science Journal, 64 (1) (2014) 48-54.
[29] H. K. Aggarwal, A. Majumdar, Single-sensor multi-spectral image demosaicing algorithm using learned interpolation weights, IEEE Int. Geosci. Remote Sens. Symp. (IGARSS), (2014) 2011–2014.

[30] X. Wang, J B. Thomas, J. Y. Hardeberg, P. Gouton, Discrete wavelet transform based multispectral filter array demosaicking, CVCS, (2013) 1–6.
[31] C. Wang, X. Wang, J. Hardeberg, A linear interpolation algorithm for spectral filter array demosaicking, Image and Signal Process. Springer Internat. Publish. 8509 (2014) 151-160.
[32] Y. Monno, D. Kiku, M. Tanaka, Adaptive residual interpolation for color and multispectral image demosaicking, Sensors 17 (12) (2017).
[33] S. Mihoubi, O. Losson, B. Mathon, L. Macaire, Multispectral demosaicing using intensity-based spectral correlation, IPTA, Image Process. Theory, (2015), 461-466.
[34] P. Amba, J. B. Thomas, D. Alleysson, N-LMMSE demosaicing for spectral filter arrays. J. Imaging Sci. Technol. 61 (2017) 40407-1–40407-11.
[35] D. Alleysson, S. Susstrunk, J. Herault, Color demosaicing by estimating luminance and opponent chromatic signals in the fourier domain, Proc. Color Imag. Conf. (2002) 331–336.
[36] N. Lian, L. Chang, Y. P. Tan, Improved color filter array demosaicking by accurate luminance estimation, IEEE, Image Process. Conf. 1 (2005).
[37] Multispectral image dataset: http://www.cs.columbia.edu/CAVE/databases/multispectral/.
[38] Y. M. Lu, C. Fredembach, M. Vetterli, S. Süsstrunk, Designing color filter arrays for the joint capture of visible and near-infrared images, IEEE Intern. Conf. on Image Proc. (2009) 3797–3800.
[39] J. Mizutani, S. Ogawa, K. Shinoda, M. Hasegawa, S. Kato, Multispectral demosaicking algorithm based on interchannel correlation, *IEEE Visual Commu. and Image Proc. Conf.* (2014) 474–477.